Claudin-2–deficient mice are defective in the leaky and cation-selective paracellular permeability properties of renal proximal tubules

Shigeaki Muto[a,1,2], Masaki Hata[b,1], Junichi Taniguchi[c], Shuichi Tsuruoka[d], Kazumasa Moriwaki[e], Mitinori Saitou[f], Kyoko Furuse[b], Hiroyuki Sasaki[b], Akio Fujimura[d], Masashi Imai[c], Eiji Kusano[a], Shoichiro Tsukita[f,3], and Mikio Furuse[g]

Departments of [a]Nephrology, [c]Pharmacology, and [d]Clinical Pharmacology, Jichi Medical University, Shimotsuke, Tochigi 329-0498, Japan; [b]KAN Research Institute, Inc., Kobe MI R&D Center, Kobe, Hyogo 650-0047, Japan; Divisions of [e]Vascular Biology and [g]Cell Biology, Department of Physiology and Cell Biology, Kobe University Graduate School of Medicine, Kobe, Hyogo 650-0017, Japan; and [f]Department of Cell Biology, Kyoto University Faculty of Medicine, Kyoto 606-8501, Japan

Edited* by Gerhard Giebisch, Yale University School of Medicine, New Haven, CT, and approved March 18, 2010 (received for review November 10, 2009)

Claudin-2 is highly expressed in tight junctions of mouse renal proximal tubules, which possess a leaky epithelium whose unique permeability properties underlie their high rate of NaCl reabsorption. To investigate the role of claudin-2 in paracellular NaCl transport in this nephron segment, we generated knockout mice lacking *claudin-2* (*Cldn2*$^{-/-}$). The *Cldn2*$^{-/-}$ mice displayed normal appearance, activity, growth, and behavior. Light microscopy revealed no gross histological abnormalities in the *Cldn2*$^{-/-}$ kidney. Ultrathin section and freeze-fracture replica electron microscopy revealed that, similar to those of wild types, the proximal tubules of *Cldn2*$^{-/-}$ mice were characterized by poorly developed tight junctions with one or two continuous tight junction strands. In contrast, studies in isolated, perfused S2 segments of proximal tubules showed that net transepithelial reabsorption of Na^+, Cl^-, and water was significantly decreased in *Cldn2*$^{-/-}$ mice and that there was an increase in paracellular shunt resistance without affecting the apical or basolateral membrane resistances. Moreover, deletion of claudin-2 caused a loss of cation (Na^+) selectivity and therefore relative anion (Cl^-) selectivity in the proximal tubule paracellular pathway. With free access to water and food, fractional Na^+ and Cl^- excretions in *Cldn2*$^{-/-}$ mice were similar to those in wild types, but both were greater in *Cldn2*$^{-/-}$ mice after i.v. administration of 2% NaCl. We conclude that claudin-2 constitutes leaky and cation (Na^+)–selective paracellular channels within tight junctions of mouse proximal tubules.

mouse proximal tubule | tight junction | paracellular transport | Na/Cl transport | water transport

Tight junctions (TJs) are circumferential seals around cells that selectively modulate paracellular permeability between extracellular compartments (1–3). On ultrathin-section electron microscopy, TJs appear as foci where the plasma membranes of neighboring cells make complete contact (4). On freeze-fracture electron microscopy, TJs appear as a continuous and anastomosing network of intramembranous particle strands (TJ strands) (5). These strands are mainly composed of linearly polymerized integral membrane proteins called claudins with molecular masses of ~23 kDa (2, 3, 6). The claudin gene family contains more than 20 members in humans and in mice (2, 3, 7). The expression pattern of claudins varies considerably; most cell types express more than two claudins in various combinations to constitute mosaic TJ strands.

Through the formation of TJ strands, claudins are directly involved in creating a primary barrier to the paracellular diffusion of solutes and water across epithelia (8). However, TJs are not a simple barrier: the barrier varies in tightness, measured by the transepithelial electrical resistance (R_T), and charge selectivity. Furuse et al. (9) reported that, when canine claudin-2 cDNA was transfected into high-resistance Madin-Darby canine kidney (MDCK) I cells primarily expressing claudins-1 and -4, the R_T decreased to a level similar to that of low-resistance MDCK II cells expressing endogenous claudins-1, -2, and -4. A similar claudin-2–induced decrease in R_T was attributed to an increase in the cation-selective permeability of TJs (10). Furthermore, the overexpression of human claudin-4 in MDCK II cells increased R_T by selectively decreasing the paracellular permeability for Na^+ without affecting that for Cl^- or an uncharged solute (11). Similarly, overexpression of claudin-8 in MDCK II cells decreased paracellular permeability to cations but not to anions or neutral solutes (12). The combination and ratios of claudins may determine the tightness and charge selectivity of individual TJ strands, and some claudin species may constitute charge-selective paracellular channels within TJ strands (9, 11, 12). This hypothesis was also proposed through analysis of human hereditary hypomagnesemia caused by mutations in claudin-16 (13). However, the results obtained from exogenous expression of claudins in cultured epithelial cells are unclear: claudin function must be investigated without knowing the exact combination and ratios of endogenous claudins, and it is not assured whether exogenous claudins form TJ strands correctly without affecting endogenous claudins. Mouse lines lacking the expression of several claudin species have been generated (14–17), but the barrier functions of their TJs have not always been evaluated by electrophysiology.

We focused on the function of claudin-2 in the kidney. Claudin-2 is highly expressed, together with other claudin isoforms such as claudin-10, in the proximal tubule of the kidney (18, 19), which is composed of a leaky epithelium (20). In the proximal tubule, approximately one-third of the NaCl reabsorption is passive via the paracellular pathway; the remainder is active via the transcellular pathway. The movement of NaCl therefore results in passive water reabsorption. In this tubule, the molecular mechanisms behind the transcellular transport of NaCl and water have been extensively evaluated, but it remains totally elusive how these molecules are transported across TJs. In this study, we generated claudin-2–deficient mice and examined whether claudin-2 is involved in the paracellular transport of NaCl and water in vivo.

Results and Discussion

We produced mice unable to express claudin-2. Nucleotide sequencing and restriction mapping identified one exon that covers the whole ORF of *claudin-2*. We constructed a targeting vector to disrupt the *claudin-2* gene by replacing part of the ORF (a.a. 1–

Author contributions: S.M., S. Tsukita, and M.F. designed research; S.M., M.H., J.T., S. Tsuruoka, K.M., M.S., K.F., H.S., and M.F. performed research; S.M., A.F., M.I., E.K., S. Tsukita, and M.F. analyzed data; and S.M., S. Tsukita, and M.F. wrote the paper.

The authors declare no conflict of interest.

*This Direct Submission article had a prearranged editor.

[1]S.M. and M.H. contributed equally to this work.

[2]To whom correspondence should be addressed. E-mail: smuto@jichi.ac.jp.

[3]Deceased December 11th, 2005.

This article contains supporting information online at www.pnas.org/cgi/content/full/0912901107/DCSupplemental.

PHYSIOLOGY

111) of claudin-2 with the neomycin resistance gene (Fig. S1*A*). Two lines of mice were generated from distinct ES cell clones in which the *claudin-2* gene was disrupted by homologous recombination. Southern blotting confirmed the expected disruption of the *claudin-2* gene (Fig. S1*B*).

Claudin-2 null [$Cldn2^{-/-}$] mice were born in the expected Mendelian ratios. Their growth rate, appearance, activity, and behavior were normal. This enabled an examination of the structure and function of proximal tubules using male adult $Cldn2^{-/-}$ mice and their wild-type littermates [$Cldn2^{+/+}$]. The two lines of $Cldn2^{-/-}$ mice showed the same phenotype, so we will present data obtained from one line of the two.

We first compared light microscopic images of H&E-stained sections of paraffin-embedded kidneys from 8-week-old $Cldn2^{+/+}$ and $Cldn2^{-/-}$ mice (Fig. S2). No gross morphological malformations were observed in the $Cldn2^{-/-}$ kidney. Ultrathin section electron microscopy also identified no significant differences between $Cldn2^{+/+}$ and $Cldn2^{-/-}$ kidneys, including in proximal tubule cells (Fig. 1*A*). Similar to $Cldn2^{+/+}$ kidneys, epithelial cells delineating $Cldn2^{-/-}$ proximal tubules were well polarized, bearing numerous microvilli on their apical surfaces and TJs at the most apical region of their lateral membranes. As previously reported (21), the TJ area was not well developed in the junctional complex in $Cldn2^{+/+}$ proximal tubules, and contained only one or two "kissing points" where plasma membranes of neighboring cells made complete contact. Interestingly, in $Cldn2^{-/-}$ proximal tubules, all epithelial cells observed also had one or two kissing points. Freeze-fracture replica electron microscopy can also identify proximal tubules by their characteristic morphology. The majority of epithelial cells of proximal tubules in $Cldn2^{+/+}$ mice possessed a single TJ strand/groove that appeared to continuously seal the paracellular space (Fig. 1*B*). All of the epithelial cells delineating $Cldn2^{-/-}$ proximal tubules also bore at least one TJ strand (Fig. 1*B*).

Next, we investigated claudin expression in proximal tubules. In our previous study (18), we reported the colocalization of claudin-2 with claudins-10 and -11 at TJs of mouse proximal tubules. However, because we now believe that our anti–claudin-11 pAb cross-reacts with claudin-10 (Fig. S3), we have not studied claudin-11 here. By immunofluorescence, claudin-2 was not detected at TJs of proximal tubules in $Cldn2^{-/-}$ kidneys, but the distribution of claudin-10 was not significantly altered (Fig. 2*A*). To investigate whether other claudins were up-regulated to compensate for the lack of claudin-2 in $Cldn2^{-/-}$ proximal tubules, we performed quantitative real-time PCR using mRNA from isolated proximal tubules. The amount of *claudin-10a* and *-10b* mRNA was not statistically different between the two groups (Fig. 2*B*). In $Cldn2^{-/-}$ proximal tubules, we did not find any significant mRNA up-regulation of any *claudin* expressed in nephron segments apart from the proximal tubule, including *-4*, *-8,* and *-16* (Fig. 2*B*). Furthermore, by immunofluorescence in $Cldn2^{-/-}$ kidneys, the claudins that were reportedly expressed in other nephron segments, including claudins-4, -8, and -16, were still undetectable at TJs of their proximal tubules (Fig. S4). In addition, ZO-1 and cingulin, proteins localized in the cytoplasmic region of TJs, colocalized with *Lotus tetragonolobus agglutinin* (LTA), a proximal tubule marker (19, 22), in $Cldn2^{-/-}$ kidneys (Fig. S5). Therefore, claudin-2 appeared to be simply absent from TJs of the proximal tubule in $Cldn2^{-/-}$ mice. Because $Cldn2^{-/-}$ proximal tubule epithelial cells possess apparently normal TJ strands, it is likely that claudin-10 replaces claudin-2, although this is difficult to prove by immunofluorescence.

In contrast to the morphology, functional studies in $Cldn2^{-/-}$ kidneys revealed striking differences from $Cldn2^{+/+}$ kidneys. Net transepithelial reabsorption of Na^+, Cl^- and water (J_{Na}, J_{Cl} and J_v, respectively) in $Cldn2^{-/-}$ proximal tubules all significantly decreased compared with that in $Cldn2^{+/+}$ proximal tubules (71.9 ± 2.4 vs. 114.9 ± 1.8 peq/mm/min, 57.5 ± 1.6 vs. 75.4 ± 1.8 peq/mm/min and 0.56 ± 0.01 vs. 0.78 ± 0.02 nl/mm/min, respectively) (Fig. 3). These findings indicate that claudin-2 is important for transepithelial reabsorption of NaCl and water in mouse proximal tubules. To determine whether the decreases in J_{Na} and J_{Cl} in $Cldn2^{-/-}$ tubules

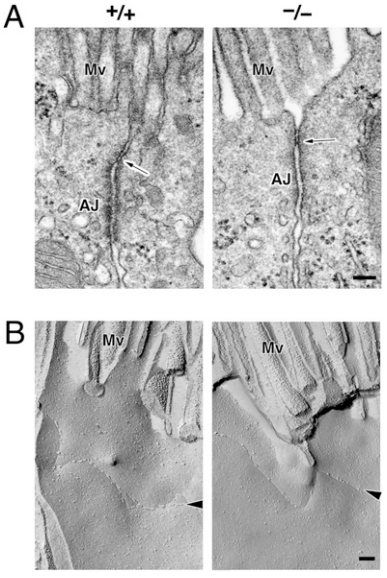

Fig. 1. Electron microscopic images of $Cldn2^{+/+}$ and $Cldn2^{-/-}$ proximal tubules. (*A*) Ultrathin section. Arrows indicate tight junctions (TJs). AJ, adherens junction; MV, microvilli. (Bars, 100 nm.) (*B*) Freeze-fracture replica. Arrowheads indicate TJ strands. MV, microvilli. (Bars, 100 nm.)

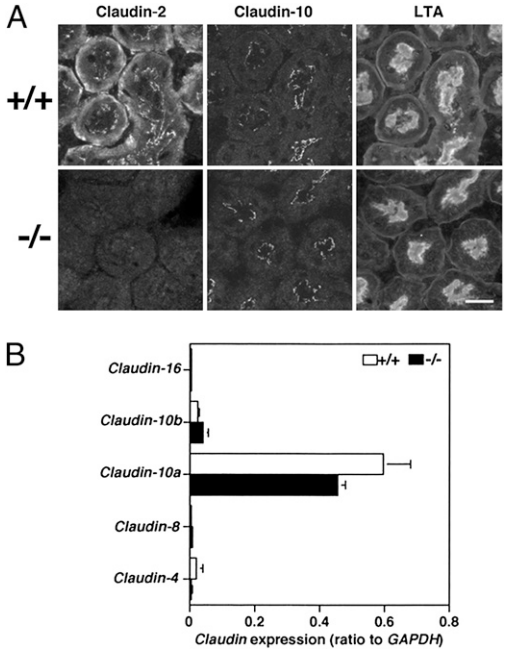

Fig. 2. Expression of claudins in the proximal tubule of $Cldn2^{+/+}$ and $Cldn2^{-/-}$ mice. (*A*) Immunolocalization of claudins-2 and -10. One of each pair of serial frozen sections was stained with anti–claudin-2 pAb (*Left Column*) and the other was stained with anti–claudin-10 pAb (*Center Column*). The same section as claudin-10 staining was also labeled with *Lotus tetragonolobus agglutinin* (LTA), a marker for the proximal tubule (*Right Column*). Proximal tubules were identified by LTA staining of their apical and basolateral membranes (19). (Bars, 20 μm.) (*B*) Quantification of mRNA levels of *claudins-4*, *-8*, *-10a*, *-10b,* and *-16* relative to *GADPH* in isolated proximal tubules of $Cldn2^{+/+}$ and $Cldn2^{-/-}$ mice (n = 4 per group).

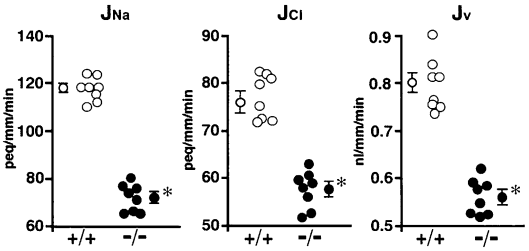

Fig. 3. Net transepithelial reabsorption of Na^+, Cl^-, and water (J_{Na}, J_{Cl}, and J_v, respectively) in isolated perfused S2 segments of proximal tubules from *Cldn2*$^{+/+}$ and *Cldn2*$^{-/-}$ kidneys. Each datapoint is from one tubule of one mouse. Averaged data ± SEM of eight *Cldn2*$^{+/+}$ and eight *Cldn2*$^{-/-}$ proximal tubules are shown at the left or right of each data set. *$P < 0.001$ vs. *Cldn2*$^{+/+}$ tubules.

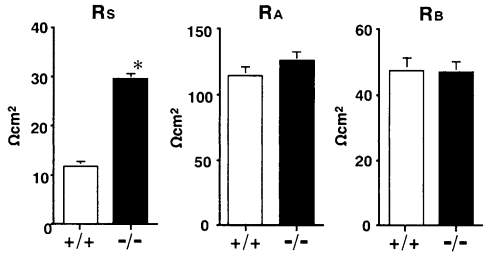

Fig. 4. Paracellular shunt resistance (R_S), apical membrane resistance (R_A), and basolateral membrane resistance (R_B) in isolated perfused S2 segments of proximal tubules from *Cldn2*$^{+/+}$ and *Cldn2*$^{-/-}$ kidneys. Values are mean ± SEM of 40 *Cldn2*$^{+/+}$ proximal tubules and 41 *Cldn2*$^{-/-}$ proximal tubules. *$P <$ 0.001 vs. *Cldn2*$^{+/+}$ tubules.

were due to increased transcellular and/or paracellular electrical resistances, we compared cable properties between the groups (Table 1). When *Cldn2*$^{+/+}$ proximal tubules were perfused with symmetrical control NaCl solutions, R_T averaged 11.3 ± 0.4 Ωcm^2, indicating that *Cldn2*$^{+/+}$ proximal tubules are leaky epithelia. In contrast, R_T in *Cldn2*$^{-/-}$ tubules was significantly higher at 25.2 ± 1.0 Ωcm^2. Fractional apical membrane resistance (fR_A), transepithelial voltage (V_T), and basolateral membrane voltage (V_B) were not different between the groups. The paracellular shunt resistance (R_S) in *Cldn2*$^{-/-}$ tubules (29.3 ± 1.3 Ωcm^2) reflected the R_T and significantly increased nearly 2.5-fold compared with that in *Cldn2*$^{+/+}$ tubules (11.6 ± 0.6 Ωcm^2), without influencing either apical or basolateral membrane resistances (R_A or R_B, respectively) (Fig. 4). Therefore, *Cldn2*$^{-/-}$ proximal tubules are indeed composed of tighter epithelia than *Cldn2*$^{+/+}$ proximal tubules. The decreases in J_{Na} and J_{Cl} in *Cldn2*$^{-/-}$ tubules are primarily attributable to impairment of net paracellular reabsorption of Na^+ and Cl^-, and the consequent inhibition of passive net paracellular water reabsorption. In the proximal tubule, most transepithelial water reabsorption likely occurs transcellularly via the aquaporin 1 channel. Thus, reduced paracellular NaCl reabsorption in the *Cldn2*$^{-/-}$ tubules may lead to a commensurate reduction in osmotically driven transcellular water reabsorption through aquaporin 1. However, in *aquaporin 1* knockout mice, proximal tubule net water reabsorption was reduced by only 50% (23), suggesting the existence of alternative pathways of water reabsorption. We found that proximal tubule net water reabsorption in *Cldn2*$^{-/-}$ mice was decreased by ≈30% compared with that in *Cldn2*$^{+/+}$ mice. Alternatively, therefore, in the proximal tubule, the claudin-2-dependent paracellular pathway may potentially contribute to the non–aquaporin 1–mediated fraction of net transepithelial water reabsorption. These possibilities await further investigation.

To estimate Na^+ permeability relative to Cl^- (P_{Na}/P_{Cl}) in proximal tubules, we observed changes in V_T when both the luminal and bathing solutions were initially a control NaCl solution, and only the luminal solution was changed to a low NaCl solution. In *Cldn2*$^{+/+}$ tubules, when the luminal perfusate was abruptly changed to the low NaCl solution, V_T deflected toward the positive (Fig. 5*A*), and the diffusion voltage (corrected for the liquid junction potential induced by reducing luminal NaCl) was +0.54 ± 0.10 mV. The P_{Na}/P_{Cl} in *Cldn2*$^{+/+}$ tubules averaged 1.10 ± 0.02 (Fig. 5*B*); this was significantly ($P < 0.001$) greater than unity, indicating a higher Na^+ permeability. In contrast, in *Cldn2*$^{-/-}$ tubules under the same conditions, V_T deflected markedly toward the negative (Fig. 5*A*); the corrected diffusion voltage was –4.57 ± 0.37 mV, and P_{Na}/P_{Cl} was 0.53 ± 0.03 (Fig. 5*B*). These results indicate that *Cldn2*$^{-/-}$ tubules are

Table 1. Electrical properties in isolated perfused S2 segments of proximal tubules from *Cldn2*$^{+/+}$ and *Cldn2*$^{-/-}$ mice

	+/+	–/–
No. of tubules	44	48
Tubular length, μm	772.4 ± 23.8	788.7 ± 20.4
Tubular radius, μm	13.0 ± 0.2	12.9 ± 0.2
R_T, Ωcm^2	11.3 ± 0.4	25.2 ± 1.0*
fR_A	0.72 ± 0.01	0.73 ± 0.01
V_T, mV	–0.91 ± 0.13	–0.62 ± 0.13
V_B, mV	–65.1 ± 1.1	–66.4 ± 1.5

Values are mean ± SEM. fR_A, fractional apical membrane resistance; R_T, transepithelial electrical resistance; V_B, basolateral membrane voltage; V_T, transepithelial voltage.
*$P < 0.001$ vs. *Cld2*$^{+/+}$ tubules.

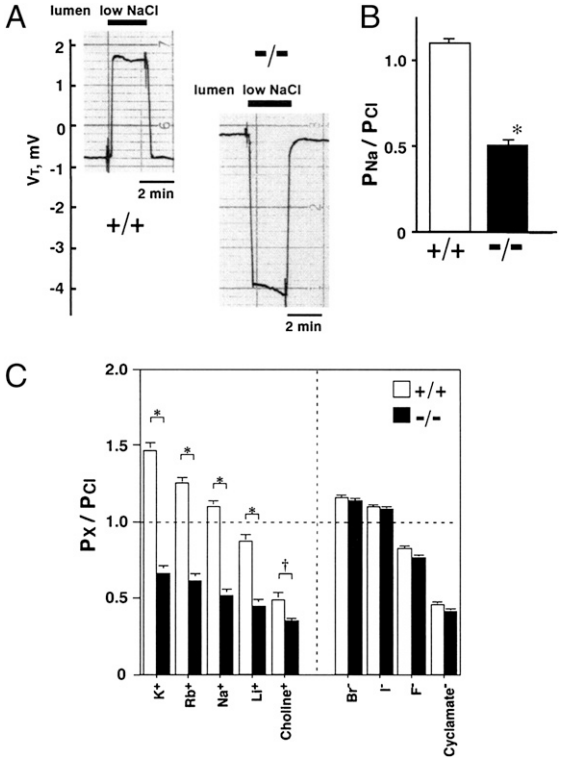

Fig. 5. Relative permeability properties in isolated perfused S2 segments of proximal tubules from *Cldn2*$^{+/+}$ and *Cldn2*$^{-/-}$ kidneys. (*A*) Representative tracings of the transepithelial voltage (V_T) on reducing luminal NaCl. (*B*) Relative permeability of Na^+ to Cl^- (P_{Na}/P_{Cl}). Values are mean ± SEM of 76 *Cldn2*$^{+/+}$ proximal tubules and 82 *Cldn2*$^{-/-}$ proximal tubules. *$P < 0.001$ vs. *Cldn2*$^{+/+}$ tubules. (*C*) Relative permeabilities of cations and anions to Cl^- (P_X/P_{Cl}). Values are mean ± SEM of 11 *Cldn2*$^{+/+}$ proximal tubules and 10 *Cldn2*$^{-/-}$ proximal tubules. *$P < 0.001$, †$P < 0.05$ vs. *Cldn2*$^{+/+}$ tubules.

relatively permeable to Cl^-. We could clearly discriminate *Cldn2*$^{-/-}$ from *Cldn2*$^{+/+}$ mice by the V_T response upon reducing luminal NaCl concentration. Inhibiting the basolateral Na^+ pump by addition of ouabain (100 μM) had no effect on P_{Na}/P_{Cl} in either group (Fig. S6), indicating a paracellular pathway of the permeability ratio. Theoretically, the decrease in P_{Na}/P_{Cl} in *Cldn2*$^{-/-}$ tubules represents a decrease in P_{Na}, an increase in P_{Cl} or a combination of both. Because the R_S was significantly greater in *Cldn2*$^{-/-}$ tubules (Fig. 4), the decrease in P_{Na}/P_{Cl} must result primarily from a decrease in P_{Na}. When Na^+ is transported, an anion, like Cl^-, must accompany it so that the electroneutrality of the fluid compartments is maintained. Accordingly, in *Cldn2*$^{-/-}$ tubules, reduction of the net paracellular Na^+ reabsorption results in an inhibition of the net paracellular Cl^- reabsorption. The *Cldn2*$^{+/+}$ tubules were also permeable to cations other than Na^+, and the sequence of their permeabilities relative to Cl^- was $K^+ > Rb^+ > Na^+ > Li^+ > choline^+$ (Fig. 5*C*). This permeability sequence is similar to that reported for leaky epithelia such as the rabbit gallbladder (24) and the rat gut (25). The *Cldn2*$^{+/+}$ tubules were also permeable to anions other than Cl^-, and the sequence of their permeabilities relative to Cl^- was $Br^- > I^- > F^- > cyclamate^-$ (Fig. 5C). In *Cldn2*$^{-/-}$ tubules, the relative permeabilities of the other cations were also significantly lower than those in *Cldn2*$^{+/+}$ tubules, but the relative permeabilities of the other anions were almost identical to those in *Cldn2*$^{+/+}$ tubules (Fig. 5*C*). These results indicate that the *Cldn2*$^{-/-}$ proximal tubules have significantly less cation selectivity, and therefore that claudin-2 creates cation-selective pores in the proximal tubule paracellular pathway with the ranking of $K^+ > Rb^+ > Na^+ > Li^+ > choline^+$. This metal cation ranking corresponds to sequence IV or V of Eisenman's 11 alkali cation sequences (26). Similarly, in claudin-2–overexpressing MDCK-C7 (10) and MDCK I (27) cells, the permeability sequence was $Na^+ = K^+ > N$-methyl-D-glucamine$^+ > choline^+ >> Cl^- = Br^-$ and $K^+ > Rb^+ > Na^+ > Li^+ >> Cs^+$, respectively.

Next, we performed metabolic balance studies to examine whether the decreases in J_{Na}, J_{Cl}, and J_v in *Cldn2*$^{-/-}$ proximal tubules influenced whole kidney electrolytes and water transport. With free access to water and food, serum levels of Na^+, K^+, Cl^-, Ca^{2+}, Mg^{2+}, inorganic phosphate (P), creatinine, or osmolality did not differ between the groups (Table S1). In addition, fractional excretions of K^+ (FE_K), Mg^{2+} (FE_{Mg}), P (FE_P), urine glucose, urine albumin, and creatinine clearance (C_{Cr}) were not different between the two groups (Table 2). In sharp contrast, it should be noted that the fractional excretion of Ca^{2+} (FE_{Ca}) was significantly greater in *Cldn2*$^{-/-}$ mice (Table 2), indicating that the *Cldn2*$^{-/-}$ mice were hypercalciuric. The proximal tubule passively reabsorbs a large fraction of filtered Ca^{2+} by the paracellular route (20). Yu et al. (27) have shown that, in MDCK I cells overexpressing claudin-2, Ca^{2+} passes through claudin-2 pores, with its permeability being approximately 4-fold lower than that of Na^+. Thus, the hypercalciuria observed in the *Cldn2*$^{-/-}$ mice may result from impaired Ca^{2+} reabsorption through the proximal tubule paracellular pathway. Therefore, claudin-2 may also form paracellular Ca^{2+} channels in the proximal tubule. Further studies will be required to investigate this hypothesis. Systolic blood pressure determined by tail-cuff plethysmography did not differ between the groups (Table S1). We expected that the decreases in J_{Na} and J_{Cl} in *Cldn2*$^{-/-}$ proximal tubules would result in increased delivery of NaCl-rich fluid into distal nephron segments and consequently enhance urinary excretions of Na^+ and Cl^-. Unexpectedly, however, neither FE_{Na} nor FE_{Cl} in *Cldn2*$^{-/-}$ mice was increased compared with those in *Cldn2*$^{+/+}$ mice (Table 2). These findings suggest that, with free access to water and food, the decreases in J_{Na} and J_{Cl} in the *Cldn2*$^{-/-}$ proximal tubules may be compensated for more distally. We therefore carried out an NaCl challenge. After i.v. administration of 2% NaCl at 20 mL/kg per hour, both FE_{Na} and FE_{Cl} were significantly greater in *Cldn2*$^{-/-}$ mice (Fig. 6), although inulin clearance in *Cldn2*$^{-/-}$ mice ($n = 6$: 7.82 ± 0.37 μL/min/g body weight and 635.1 ± 26.3 μL/min/g kidney weight) did not differ significantly from that in *Cldn2*$^{+/+}$ mice ($n = 6$: 8.94 ± 0.41 μL/min per gram body weight and 695.0 ± 39.5 μL/min per gram kidney weight). Thus, *Cldn2*$^{-/-}$ mice exhibited an exaggerated urinary NaCl loss in response to the NaCl challenge.

With free access to water and food, daily urine volume and osmolality were significantly greater and less in *Cldn2*$^{-/-}$ mice than in *Cldn2*$^{+/+}$ mice, respectively, although daily water or food intake, or body weight were not different between the groups (Table 2). These results suggest that *Cldn2*$^{-/-}$ mice may be unable to concentrate urine effectively. Even if this is so, it is probably not a consequence of proximal tubule dysfunction, because the decreases in J_{Na} and J_{Cl} in the *Cldn2*$^{-/-}$ proximal tubule were completely compensated for more distally. The abnormality may instead result from a dysfunction of the thin descending limb of Henle, because claudin-2 is also expressed at TJs of this nephron segment (18), which is composed of a leaky epithelium (28) and is important in the concentration of urine (20). This will be clarified in future studies.

It had already been reported that overexpression of claudin-2 in MDCK cells altered both tightness (9) and paracellular charge selectivity (10). However, the role of claudin-2 in these barrier functions had not been explored in intact epithelial cells. This study now demonstrates that, when just one of claudins expressed at TJs of the proximal tubule, claudin-2, was genetically disrupted in mice, both electrical resistance and cation (Na^+) selectivity in the proximal tubule paracellular pathways were markedly affected. This resulted in an impairment of their net transepithelial reabsorption of Na^+, Cl^-, and water, despite our electron microscopy studies that showed no gross differences in TJ architecture.

Table 2. Metabolic balance data in *Cldn2*$^{+/+}$ and *Cldn2*$^{-/-}$ mice

	+/+	−/−
No. of animals	10	10
BW, g	28.2 ± 0.7	28.4 ± 0.4
Water intake, μL/24 h per gram BW	200.1 ± 28.0	248.8 ± 31.5
Food intake, μg/24 h per gram BW	155.8 ± 21.2	176.8 ± 16.7
Urine volune, μL/24 h per gram BW	58.1 ± 6.8	100.8 ± 17.9*
FENa, %	0.28 ± 0.03	0.32 ± 0.02
FEK, %	25.9 ± 3.9	24.6 ± 2.1
FECl, %	0.63 ± 0.07	0.58 ± 0.05
FEMg, %	4.5 ± 0.5	4.8 ± 0.7
FECa, %	0.13 ± 0.01	0.40 ± 0.04**
FEP, %	9.2 ± 1.0	11.5 ± 1.1
Urine glucose, mg/mg cr	1.43 ± 0.12	1.48 ± 0.34
Urine albumin, μg/mg cr	7.6 ± 1.4	7.1 ± 1.2
Urine osmolality, mOsm/kgH_2O	2,499.1 ± 128.6	2,000.4 ± 125.4*
Ccr, mL/24 h per gram BW	21.5 ± 2.1	23.3 ± 1.7

Values are mean ± SEM. BW, body weight; Ccr, creatinine clearance; FE, fractional excretion.
*$P < 0.05$, **$P < 0.001$ vs. *Cldn2*$^{+/+}$ mice.

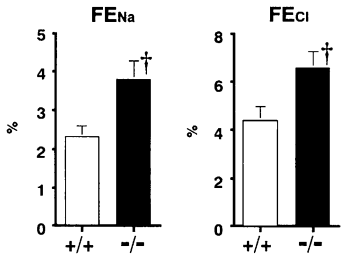

Fig. 6. Fractional excretions of Na^+ and Cl^- (FE_{Na} and FE_{Cl}, respectively) in *Cldn2*$^{+/+}$ and *Cldn2*$^{-/-}$ mice given 2% NaCl solution i.v. at 20 mL/kg per hour. Values are mean ± SEM of six *Cldn2*$^{+/+}$ and six *Cldn2*$^{-/-}$ mice. †$P < 0.05$ vs. *Cldn2*$^{+/+}$ mice.

These functional abnormalities do not result, therefore, from gross changes in TJ structure, but from the lack of claudin-2 itself. In other words, we conclude that claudin-2 determines both tightness and paracellular cation (Na^+) selectivity in mouse proximal tubules, and plays important roles in proximal tubule paracellular NaCl and water reabsorption.

Materials and Methods

Generation of Claudin-2–Deficient Mice. The targeting vector is shown in Fig. S1*A*. The diphtheria toxin A expression cassette (MC1pDT-A) was placed outside the 3′ arm of homology for negative selection. J1 ES cells were electroporated with the targeting vector and G418-resistant colonies were screened by Southern blotting with the 3′ external probe (Fig. S1*A*). Correctly targeted ES cells were injected into C57BL/6 blastocysts, which were transferred into BALB/c foster mothers to obtain chimeric mice. Male chimeras were mated with C57BL/6 females, and heterozygous mice were present in the agouti offspring. The ethics of all animal experiments were approved by the Animal Care and Use Committee of Jichi Medical University and Kyoto University.

Separation of Proximal Tubule S2 Segments, RNA Extraction, and Real-Time PCR. Single proximal tubule S2 segments were dissected from freshly killed–mouse kidney with fine forceps under a stereomicroscope at 4–5 °C. Approximately 50 tubules (length ~0.5 mm) were pooled for each sample and stored in RNAlater solution (Sigma). Total RNA was extracted from the single S2 segments using a commercial kit (Qiagen). First-strand cDNA was synthesized using an RNA PCR Kit (AMV) Ver. 3.0 (Takara) according to the manufacturer's instructions. Quantitative real-time PCR was performed using an ABI PRISM 7000 real-time PCR system and SYBR Green master mix (Applied Biosystems) with the primers for *claudins-4*, *-8*, *-10a*, *-10b,* and *-16* and *GAPDH* indicated in Table S2. Expression levels were normalized to *GAPDH* levels.

Morphological Analyses. Light and immunofluorescence microscopy, ultrathin-section electron microscopy, and freeze-fracture replica electron microcopy were performed as described previously (15, 17).

In Vitro Microperfusion Studies of Isolated Proximal Tubule S2 Segments. ***Isolation and perfusion of tubules.*** Proximal tubule S2 segments, which comprise the late portion of the proximal convoluted tubule and the early portion of the proximal straight tubule, were microdissected, mounted on glass pipettes, and perfused in vitro in a rapid-exchange chamber at 37 °C as previouisly described (28–30). The control NaCl solution in the lumen and bath comprised (in mM): 110 NaCl, 5 KCl, 25 $NaHCO_3$, 0.8 Na_2HPO_4, 0.2 NaH_2PO_4, 10 sodium acetate, 1.8 $CaCl_2$, 1.0 $MgCl_2$, 8.3 *d*-glucose, and 5 *L*-alanine. For flux studies, proximal tubules were perfused with an identical solution, except that the bath solution contained neutral dextran (20 g/L). For estimation of P_{Na}/P_{Cl}, we prepared low NaCl solution, in which 50 mM NaCl was replaced with equiosmolar sucrose (93 mM). All solutions were 285–295 mOsm/kg/H_2O osmolality, and were equilibrated with 95% O_2/5% CO_2 to adjust to pH 7.4 at 37 °C.

Measurements of J_{Na}, J_{Cl}, and J_v. J_{Na}, J_{Cl}, and J_v were measured in the isolated perfused proximal tubules using standard techniques (31). The luminal flow rate was adjusted to 8–9 nL/min by regulating the hydrostatic perfusion pressure. Each net flux was measured three times and averaged.

Electrical measurements. To measure R_T and fR_A [$fR_A = R_A/(R_A + R_B)$], in isolated perfused proximal tubules, we applied cable analysis as previously described (28–30). The perfusion pipette was double-barreled: one barrel was used for constant current injection (100 nA), whereas the second barrel was used for measuring V_T. Proximal tubule cells were impaled with conventional microelectrodes across the basolateral membrane to measure V_B (28–30). In accordance with Reuss and Finn (32), we also estimated R_A, R_B and R_S by measuring R_T and fR_A in the absence and presence of bath Ba^{2+} (1 mM), that selectively inhibits K^+ conductance (28–30, 33).

Measurements of relative permeabilities for Cl^-. Relative permeabilities for Cl^- in the isolated perfused proximal tubules were calculated from the observed transepithelial diffusion voltages according to the Goldman-Hodgkin-Katz equation, as described previously (34). Substitution of 50 mM Na^+ or Cl^- of the control NaCl solution in the lumen by other cations or anions produced bi-ionic potentials from which the relative permeabilities were calculated. The liquid junction potential induced by reducing luminal NaCl was corrected with free-flowing 3 M KCl electrodes as described previously (30).

Metabolic Balance Studies. Mice were placed in metabolic cages for 24 h and were provided a standard rodent chow and water ad libitum. We measured daily water consumption, urine volume, and food intake. After urine sample collection, blood was taken from the inferior vena cava. Urine and serum chemistries were measured with an autoanalyzer (Hitachi-7600, Hitachi Instruments). Osmolalities in serum and urine were measured by freezing-point depression osmometry (One-Ten Osmometer, Fiske). Creatinine levels in serum and urine were measured by an enzymatic method using an autoanalyzer (Hitachi-7600). In this protocol, creatinine clearance was used as a measure of the glomerular filtration rate (GFR).

NaCl Challenge Test. Mice were anesthetized with sodium pentobarbital (50 mg/kg), and were placed on a thermostatically controlled surgical table to maintain body temperature at 38–40 °C. The tail vein was cannulated for infusion of heparin (500 IU/kg), followed by continuous infusion of 2% (wt/vol) NaCl solution containing 2.5% (wt/vol) inulin at 20 mL/kg per hour throughout the experiment. After a 90-min equilibration period, urine was collected from the bladder for 30 min, and blood was then taken from the right ventricle. The concentrations of Na^+ and Cl^- were measured as above. The concentration of inulin was measured with the Anthrone method (35). Inulin clearance was used as a marker of GFR.

Data Analysis. Data are expressed as mean ± SEM. Statistical significance was estimated with Student's *t* tests. *P* values <0.05 were considered significant.

ACKNOWLEDGMENTS. We thank Dr. Gerhard Giebisch for helpful advice on an early version of the manuscript. This work was funded by Grants-in-Aid from the Ministry of Education, Science, Culture, Sports, Science and Technology of Japan and by a grant from the Salt Science Foundation.

1. Anderson JM (2001) Molecular structure of tight junctions and their role in epithelial transport. *News Physiol Sci* 16:126–130.
2. Tsukita S, Furuse M, Ito M (2001) Multifunctional strands in tight junctions. *Nat Rev Mol Cell Biol* 2:285–293.
3. Van Itallie CM, Anderson JM (2004) The molecular physiology of tight junction pores. *Physiology (Bethesda)* 19:331–338.
4. Farquhar MG, Palade GE (1965) Cell junctions in amphibian skin. *J Cell Biol* 26: 263–291.
5. Staehelin LA (1974) Structure and function of intercellular junctions. *Int Rev Cytol* 39: 191–283.
6. Furuse M, Fujita K, Hiiragi T, Fujimoto K, Tsukita S (1998) Claudin-1 and -2: Novel integral membrane proteins localizing at tight junctions with no sequence similarity to occludin. *J Cell Biol* 141:1539–1550.
7. Morita K, Furuse M, Fujimoto K, Tsukita S (1999) Claudin multigene family encoding four-transmembrane domain protein components of tight junction strands. *Proc Natl Acad Sci USA* 96:511–516.
8. Sonoda N, et al. (1999) *Clostridium perfringens* enterotoxin fragment removes specific claudins from tight junction strands: Evidence for direct involvement of claudins in tight junction barrier. *J Cell Biol* 147:195–204.
9. Furuse M, Furuse K, Sasaki H, Tsukita S (2001) Conversion of zonulae occludentes from tight to leaky strand type by introducing claudin-2 into MDCK I cells. *J Cell Biol* 153: 263–272.
10. Amasheh S, et al. (2002) Claudin-2 expression induces cation-selective channels in tight junctions of epithelial cells. *J Cell Sci* 115:4969–4976.
11. Van Itallie C, Rahner C, Anderson JM (2001) Regulated expression of claudin-4 decreases paracellular conductance through a selective decrease in sodium permeability. *J Clin Invest* 107:1319–1327.
12. Yu ASL, Enck AH, Lencer WI, Schneeberger EE (2003) Claudin-8 expression in MDCK cells augments the paracellular barrier to cation permeation. *J Biol Chem* 278: 17350–17359.
13. Simon DB, et al. (1999) Paracellin-1, a renal tight junction protein required for paracellular Mg^{2+} resorption. *Science* 285:103–106.
14. Gow A, et al. (1999) CNS myelin and sertoli cell tight junction strands are absent in Osp/claudin-11 null mice. *Cell* 99:649–659.
15. Furuse M, et al. (2002) Claudin-based tight junctions are crucial for the mammalian epidermal barrier: A lesson from claudin-1-deficient mice. *J Cell Biol* 156:1099–1111.
16. Nitta T, et al. (2003) Size-selective loosening of the blood-brain barrier in claudin-5-deficient mice. *J Cell Biol* 161:653–660.
17. Miyamoto T, et al. (2005) Tight junctions in Schwann cells of peripheral myelinated axons: A lesson from claudin-19-deficient mice. *J Cell Biol* 169:527–538.
18. Kiuchi-Saishin Y, et al. (2002) Differential expression patterns of claudins, tight junction membrane proteins, in mouse nephron segments. *J Am Soc Nephrol* 13: 875–886.
19. Enck AH, Berger UV, Yu AS (2001) Claudin-2 is selectively expressed in proximal nephron in mouse kidney. *Am J Physiol Renal Physiol* 281:F966–F974.
20. Mount DB, Yu ASL (2008) Transport of inorganic solutes: Sodium, chloride, potassium, magnesium, calcium, and phosphate. *Brenner and Rector's The Kidney*, ed Brenner BM (Saunders, Philadelphia), 8th Ed, pp 156–213.

21. Claude P (1978) Morphological factors influencing transepithelial permeability: A model for the resistance of the *zonula occludens*. *J Membr Biol* 39:219–232.
22. Laitinen L, Virtanen I, Saxén L (1987) Changes in the glycosylation pattern during embryonic development of mouse kidney as revealed with lectin conjugates. *J Histochem Cytochem* 35:55–65.
23. Schnermann J, et al. (1998) Defective proximal tubular fluid reabsorption in transgenic aquaporin-1 null mice. *Proc Natl Acad Sci USA* 95:9660–9664.
24. Moreno JH, Diamond JM (1974) Discrimination of monovalent inorganic cations by "tight" junctions of gallbladder epithelium. *J Membr Biol* 15:277–318.
25. Munck BG, Schultz SG (1974) Properties of the passive conductance pathway across *in vitro* rat jejunum. *J Membr Biol* 16:163–174.
26. Diamond JM, Wright EM (1969) Biological membranes: The physical basis of ion and nonelectrolyte selectivity. *Annu Rev Physiol* 31:581–646.
27. Yu AS, et al. (2009) Molecular basis for cation selectivity in claudin-2-based paracellular pores: Identification of an electrostatic interaction site. *J Gen Physiol* 133: 111–127.
28. Yoshitomi K, Koseki C, Taniguchi J, Imai M (1987) Functional heterogeneity in the hamster medullary thick ascending limb of Henle's loop. *Pflugers Arch* 408:600–608.
29. Muto S, Yasoshima K, Yoshitomi K, Imai M, Asano Y (1990) Electrophysiological identification of α- and β-intercalated cells and their distribution along the rabbit distal nephron segments. *J Clin Invest* 86:1829–1839.
30. Muto S, Ebata S, Asano Y (1994) Short-term effects of uninephrectomy on electrical properties of the cortical collecting duct from rabbit remnant kidneys. *J Clin Invest* 93: 286–296.
31. Matsumoto N, et al. (2003) Expression of an artificial Cl^- channel in microperfused renal proximal tubules. *J Membr Biol* 193:195–200.
32. Reuss L, Finn AL (1974) Passive electrical properties of toad urinary bladder epithelium. Intercellular electrical coupling and transepithelial cellular and shunt conductances. *J Gen Physiol* 64:1–25.
33. Völkl H, Geibel J, Greger R, Lang F (1986) Effects of ouabain and temperature on cell membrane potentials in isolated perfused straight proximal tubules of the mouse kidney. *Pflugers Arch* 407:252–257.
34. Takahashi M, Taniguchi J, Muto S, Tsuruoka S, Imai M (1999) Effect of protamine on ion selectivity of superficial and juxtamedullary proximal straight tubules. *Nephron* 83:154–159.
35. Davidson WD, Sackner MA (1963) Simplification of the anthrone method for the determination of inulin in clearance studies. *J Lab Clin Med* 62:351–356.